Molecular Therapy
Oncolytics
Original Article

Oncolytic measles vaccines encoding PD-1 and PD-L1 checkpoint blocking antibodies to increase tumor-specific T cell memory

Rūta Veinalde,[1,8] Gemma Pidelaserra-Martí,[1,2,3] Coline Moulin,[2,4] Lara M. Jeworowski,[1,9] Linda Küther,[2] Christian J. Buchholz,[5] Dirk Jäger,[6,7] Guy Ungerechts,[1,6] and Christine E. Engeland[1,2,6]

[1]Clinical Cooperation Unit Virotherapy, German Cancer Research Center, Im Neuenheimer Feld 242, 69120 Heidelberg, Germany; [2]Faculty of Health, School of Medicine, Center for Biomedical Research and Education, Institute of Virology and Microbiology, Witten/Herdecke University, Stockumer Str. 10, 58453 Witten, Germany; [3]Faculty of Biosciences, Heidelberg University, 69120 Heidelberg, Germany; [4]Ecole Normale Supérieure de Lyon, 15 parvis René Descartes, 69342 Lyon, France; [5]Molecular Biotechnology and Gene Therapy, Paul-Ehrlich-Institut, Paul-Ehrlich-Str. 51-59, 63225 Langen, Germany; [6]Department of Medical Oncology, University Hospital Heidelberg, Im Neuenheimer Feld 460, 69120 Heidelberg, Germany; [7]Clinical Cooperation Unit Applied Tumor Immunity, German Cancer Research Center, Im Neuenheimer Feld 460, 69120 Heidelberg, Germany

PD-1/PD-L1 checkpoint blockade has achieved unprecedented success in cancer immunotherapy. Nevertheless, many immune-excluded tumors are resistant to therapy. Combination with oncolytic virotherapy may overcome resistance by inducing acute inflammation, immune cell recruitment, and remodeling of the tumor immune environment. Here, we assessed the combination of oncolytic measles vaccine (MV) vectors and PD-1/PD-L1 blockade. In the MC38cea model of measles virus oncolysis, MV combined with anti-PD-1 and MV vectors encoding anti-PD-1 or anti-PD-L1 antibodies achieved modest survival benefits compared with control MV or vectors encoding the antibody constant regions only. Analyses of tumor samples and tumor-draining lymph nodes revealed slight increases in intratumoral T cell effector cytokines as well as a shift toward an effector memory phenotype in the T cell compartment. Importantly, increased IFN-γ recall responses were observed in tumor rechallenge experiments with mice in complete tumor remission after treatment with MV encoding anti-PD-1 or anti-PD-L1 compared with control MV. These results prompted us to generate MV encoding the clinically approved agents pembrolizumab and nivolumab. Previously, we have generated MV encoding atezolizumab. We demonstrated the functionality of the novel vectors *in vitro*. We envision these vectors as therapeutics that induce and support durable anti-tumor immune memory.

INTRODUCTION

The discovery of molecules that inhibit immune cell activation and the development of the immune checkpoint concept provided a basis for successful cancer immunotherapy strategies.[1,2] Programmed cell death protein 1 (PD-1 or CD279) is an immune checkpoint molecule that is upregulated on T cells upon T cell receptor (TCR) engagement and mediates peripheral immune tolerance. Besides activated T cells, PD-1 can be expressed on other types of immune cells, including natural killer (NK) cells, NKT cells, B cells and some populations of antigen-presenting cells (APCs), and even cancer cells. In many types of cancer, expression of PD-1 or its ligands programmed cell death ligand 1 (PD-L1 or CD274) and PD-L2 (CD273) is sustained at high levels.[3] PD-1/PD-L1 blockade with monoclonal antibodies has proved to be a successful therapeutic strategy to reinvigorate anti-tumor immunity.[4] Six different monoclonal antibodies for PD-1/PD-L1 blockade have been approved by the U.S. Food and Drug Administration (FDA) and the European Medicines Agency (EMA) for treatment of a range of different cancer types.[5] Although PD-1/PD-L1 blocking antibodies can achieve impressive therapeutic effects in some individuals, at least half of treated patients do not respond to therapy.[2] A major factor for resistance to PD-1/PD-L1 blockade is lack of intratumoral T cells.[6,7] Therefore, combination with agents that remodel an immunosuppressive tumor environment and recruit T cells to the tumor could alleviate this issue. Furthermore, in line with the physiological role of PD-1/PD-L1 in maintenance of immunological self-tolerance, autoimmune adverse events are frequently observed upon systemic treatment with immune checkpoint blocking antibodies.[8]

Oncolytic viruses (OV) are gaining clinical relevance as a modality of cancer immunotherapy. OVs exert therapeutic activity by specifically infecting and destroying malignant cells and by activating anti-tumor immune responses. OV infection induces an acute inflammation

Received 31 August 2021; accepted 27 November 2021;
https://doi.org/10.1016/j.omto.2021.11.020.

[8]Present address: IQVIA Biotech, 1001 Riga, Latvia

[9]Present address: Institute of Virology, Charité-Universitätsmedizin Berlin, Corporate Member of Freie Universität Berlin, Humboldt-Universität zu Berlin, and Berlin Institute of Health and German Centre for Infection Research (DZIF), Charitéplatz 1, 10117 Berlin, Germany

Correspondence: Christine E. Engeland, MD, PhD
E-mail: christine.engeland@uni-wh.de

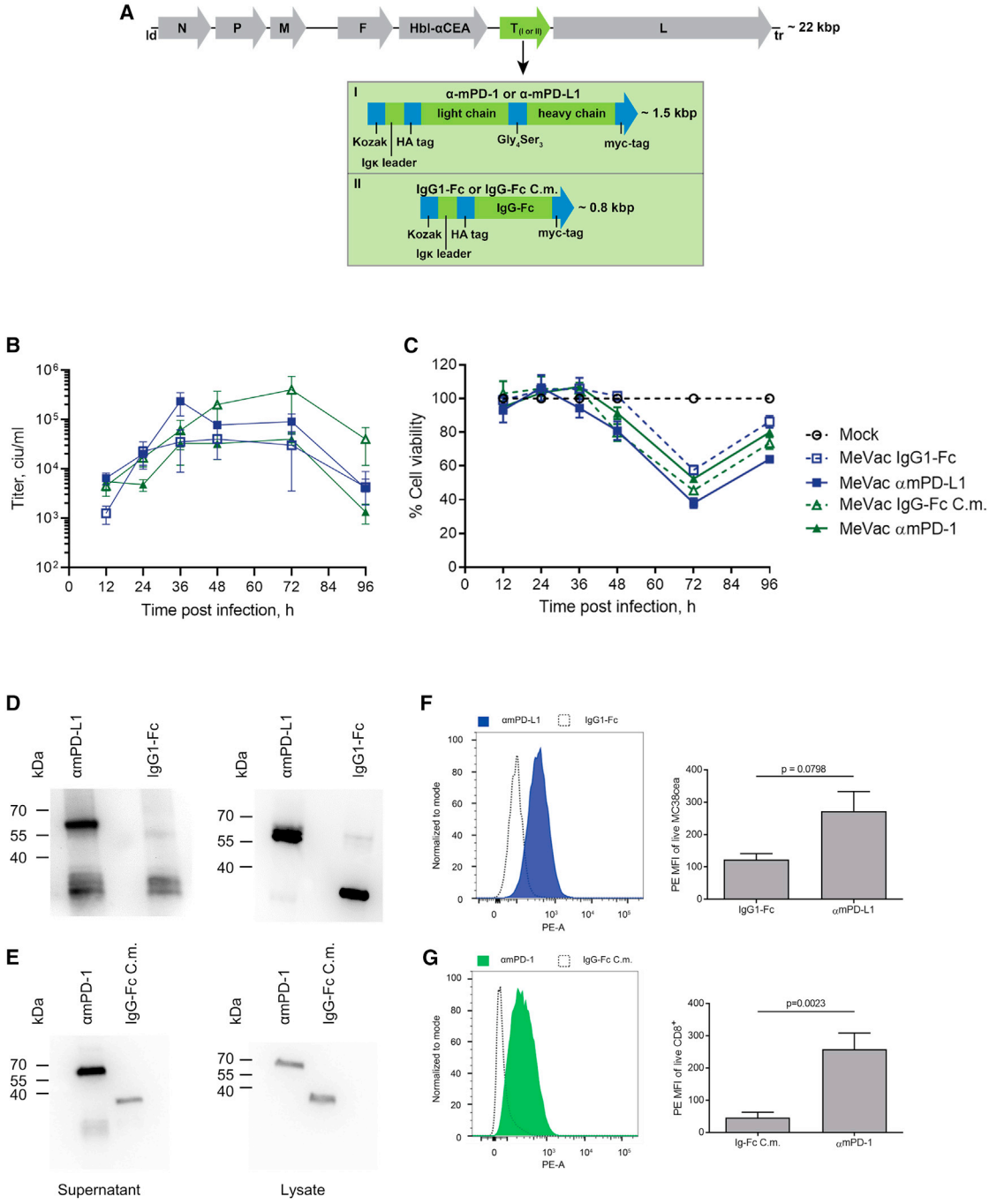

Figure 1. MeVac encoding antibodies against murine PD-1 and PD-L1

(A) Vector design. Schematic of MeVac vectors encoding the respective transgenes (T). Transgene cassettes include a Kozak sequence, mouse immunoglobulin κ secretion signal, HA and myc tags for detection, and the respective light and heavy chains of antibodies targeting murine PD-1 and PD-L1 connected by a glycine-serine linker. Transgene cassettes including the respective Fc fragments only were used for controls. To target murine MC38cea tumors, the natural tropism of the MeVac vectors was modified by fusing a single chain variable fragment of a CEA-specific antibody to "blinded" measles H with mutations in the receptor binding sites (Hbl-αCEA). N, P, M, F, and L, genes encoding measles structural proteins; ld, measles virus leader; tr, measles virus trailer. (B) Replication kinetics. MC38cea cells were infected with MeVac vectors encoding the respective transgenes at a multiplicity of infection (MOI) of 3. Triplicate samples were pooled, and viral progeny at designated time points were determined by titration assay in cell infectious units (ciu) per milliliter cell culture supernatant. Mean values of quadruplicates are shown. Error bars indicate SD. (C) Cell viability. MC38cea cells were infected with MeVac vectors encoding the respective transgenes at MOI = 5. Cell viability was determined using XTT assay at the depicted time points. Results are

(legend continued on next page)

within the tumor and provides pathogen- and danger-associated molecular patterns. Death of OV-infected tumor cells releases tumor-associated antigens (TAAs) in this immunostimulatory context, thereby promoting immune cell influx, anti-tumor immune responses and remodeling of the tumor immune environment.[9] During OV infection, expression of peripheral immune checkpoint molecules PD-L1 and PD-1 is also upregulated, creating a potential resistance to the therapy.[10,11] Thus, OV therapy and PD-1/PD-L1 blockade may complement and potentiate each other by synergistic mechanisms of action. Combination therapy may increase the range of responsive tumors, as each therapy would target a resistance factor of the other. Multiple studies have demonstrated that combination of an oncolytic virus and PD-1/PD-L1 blockade provides therapeutic benefits.[10–14] A phase Ib clinical study combining intratumoral injections of the clinically approved OV talimogene laherparepvec (T-VEC) and systemic administration of pembrolizumab demonstrated that the combination is well tolerated and provides high overall and complete response rates in advanced melanoma.[15] Correlative research indicated that T-VEC therapy remodels the tumor environment in favor of further PD-1 blockade.[16] Several variables affect the efficacy of a combination therapy regimen, including the sequencing schedule of the therapies, choice of the specific PD-1/PD-L1 antibody, and choice of OV platform. At least ten different OV platforms have been investigated as potential partners for PD-1/PD-L1 blockade in pre-clinical and clinical studies.[17] Currently there are insufficient data to ascertain which combination strategy provides optimal efficacy.

Among these OV platforms, oncolytic measles virus (MV) vectors, based on attenuated measles vaccine strain viruses, are characterized by their solid safety record, efficacious cytotoxicity mechanism, and versatility. Numerous pre-clinical studies[18] and early clinical data[19–23] indicate efficacy against a range of tumor entities. The MV vector platform can be used to encode large transgenes, including monoclonal antibodies.[18] We have previously demonstrated that oncolytic MV encoding anti-human/murine-PD-L1 (atezolizumab) provides higher therapeutic efficacy in pre-clinical murine tumor models in comparison with control MV vectors.[12,24]

In this study we aimed to investigate options for the combination of oncolytic MV vectors with PD-1/PD-L1 blockade in more detail. Using the MV Schwarz vaccine platform (MeVac), we developed novel vectors encoding PD-1 blocking antibodies. We compared these novel vectors with the previously developed anti-PD-L1 encoding vector. Furthermore, we assessed whether the combination of oncolytic MeVac with systemically or vector-encoded PD-1/PD-L1 checkpoint blockade was more effective. Correlative analyses indicated a more robust T cell memory response by the combination of MeVac and PD-1/PD-L1 blockade compared with MeVac alone. On the basis of our results, we developed MeVac vectors encoding the clinically approved PD-1 blocking antibodies nivolumab and pembrolizumab.

RESULTS

Tumor cell expression of PD-L1 after oncolytic measles virus treatment

Studies from our and other groups had previously reported upregulation of PD-L1 upon virotherapy.[12,25,26] We confirmed this finding in murine tumor cell lines. 48h after inoculation with MeVac, B16-CD46 melanoma and MC38-CD46 colorectal adenocarcinoma cells showed upregulation of PD-L1 compared with mock infected controls (Figure S1). Upregulation of PD-L1 upon virotherapy may sensitize tumors to PD-1/PD-L1 checkpoint blockade or represent a possible resistance mechanism. Therefore, this finding provides a rationale for testing the combination of virotherapy with PD-1/PD-L1 checkpoint blockade.

Generation and *in vitro* characterization of a novel MeVac vector encoding an antibody against murine PD-1

We have previously described a MeVac vector encoding an antibody against murine and human PD-L1, MeVac αmPD-L1, wherein the antibody sequence corresponds to the clinically used agent atezolizumab.[12] In analogy to this vector, we generated a vector encoding an antibody against murine PD-1, MeVac αmPD-1. The cassettes for αmPD-1 and αmPD-L1 consist of the light and heavy chains of the respective antibodies linked by a glycine-serine linker, preceded by a Kozak sequence and an Igκ leader sequence as a secretion signal. HA and myc tags are included in the constructs for detection and purification of the encoded antibodies (Figure 1A). The anti-PD-L1 antibody is of human IgG1 subtype, which can interact with murine Fc receptors and mediate antibody-dependent cellular cytotoxicity (ADCC).[27] The novel αmPD-1 construct encompasses an Fc region from Syrian hamster (*Cricetulus migratorius* [*C.m.*]), corresponding to the antibody used for systemic PD-1 blockade. As controls, vectors encoding the respective Fc regions only were generated (MeVac IgG1-Fc and MeVac IgG-Fc *C.m.*).

Cassettes encoding the transgenes were inserted into the MeVac genome downstream of the MeVac hemagglutinin (H) open reading frame, as depicted in Figure 1A. Murine cells are not susceptible to MeVac, because of the lack of the respective cell entry receptors. To allow investigation of these vectors in the established murine

depicted as percentage viable cells compared with mock at the respective time point. Mean values of triplicates are shown. Error bars indicate SD. (D and E) Secretion of MeVac-encoded antibodies from infected cells. MC38cea cells were infected with MeVac encoding the respective transgenes at MOI = 3. Supernatants were collected at 48 h post-infection and analyzed by western blot using an antibody specific for the HA tag. (F and G) Binding of MeVac-encoded antibodies. (F) MC38cea tumor cells that express PD-L1 were incubated with supernatants collected from Vero-αHis cells infected with MeVac encoding αmPD-L1 or IgG1-Fc and stained with a PE-labeled antibody against the HA tag. (G) Murine cytotoxic T cells (CTL-ova) with PD-1 surface expression were incubated with supernatants collected from Vero-αHis cells infected with MeVac encoding αmPD-1 or IgG-Fc *C.m.* and stained with a PE-labeled antibody against the HA tag. Histograms showing intensity of PE signal on live cells in a representative flow cytometry experiment (left) and data summarizing the median fluorescence intensity (MFI) of PE on live cells in three independent experiments (right) are shown. Error bars indicate SD. MFI values were analyzed using unpaired t test.

MC38cea model of measles virotherapy,[28] the MeVac H attachment protein was fused to a single chain variable fragment of an antibody against human carcinoembryonic antigen (CEA).[29]

We compared the characteristics of the novel MeVac vectors encoding αmPD-1 and IgG-Fc *C.m.* with the existing constructs encoding αmPD-L1 and IgG1-Fc. Replication kinetics and cytotoxic properties in MC38cea cells as assessed by one-step growth curves and cell viability assays (Figures 1B and 1C) show similar kinetics between the different constructs. However, MeVac αmPD-1 was attenuated compared with the respective control vector, MeVac IgG Fc *C.m.*, as indicated by a more than 1 log difference in viral progeny. Secretion of αmPD-1 and αmPD-L1 after infection of MC38cea and Vero-αHis cells with the recombinant MeVac vectors was confirmed by western blot (Figures 1D, 1E, and S2). Kinetics of transgene expression were analyzed using western blot (Figure S2). High amounts of transgene product were present in input virus suspensions (time point 0 h post-infection [p.i.]). Nevertheless, these results indicate de novo synthesis of αmPD-1, αmPD-L1, IgG-Fc *C.m.*, and IgG1-Fc, with peaks at 72 h p.i. (for αmPD-1), 24–48 h p.i. (for IgG-Fc *C.m.*), and 48 h p.i. (for αmPD-L1 and IgG1-Fc).

αmPD-1 and αmPD-L1 secreted from infected cells were shown to bind PD-1-positive murine cytotoxic T cells (CTL-ova) and PD-L1-positive tumor cells, respectively (Figures 1F and 1G). Specific binding to PD-1 and PD-L1, respectively, was confirmed by competitive binding assays (Figure S3). Functionality of MeVac-encoded αmPD-L1 has also been reported previously.[24]

Therapeutic efficacy of intratumoral MeVac αmPD-1 in comparison with combination of intratumoral MeVac and systemic αmPD-1

We compared the efficacy of the novel MeVac αmPD-1 to a combination of systemic delivery of αmPD-1 and intratumoral (i.t.) therapy with MeVac IgG-Fc *C.m.* and to each of the monotherapies (MeVac IgG-Fc *C.m.* i.t. and αmPD-1 only). We tested these therapeutic strategies in the murine colorectal adenocarcinoma model MC38cea, which is syngeneic to C57BL/6 mice. MC38cea cells were implanted subcutaneously (s.c.) into the right flank of mice. After tumor establishment, mice were treated with i.t. injections of MeVac variants on 4 consecutive days according to the experimental schedule in Figure 2A. MeVac IgG-Fc *C.m.* was used as a control vector in the MeVac i.t.-only group and in the combination group of MeVac i.t. with systemic αmPD-1. In the groups that received systemic antibody treatment, intraperitoneal (i.p.) injections with the antibody were initiated on day 6 after implantation of the tumor cells and continued every third day for a total of four injections (Figure 2A). Intraperitoneal injections of αmPD-1 only did not significantly improve survival in comparison with mock treatment (Figure 2B), although there was a slight delay in tumor progression in individual animals in the αmPD-1 i.p. group (Figures 2C and 2D). In both MeVac IgG-Fc *C.m.* treatment groups, survival of the animals was significantly improved in comparison with mock treatment (Figure 2B). There were no statistically significant differences between the treatment groups that received MeVac in any of the tested regimens. Several mice in the MeVac treatment groups showed complete tumor remissions (CRs), distributed as follows: five CRs in the MeVac IgG-Fc *C.m.* i.t. and αmPD-1 i.p. combination group, four CRs in the MeVac αmPD-1 i.t. group, and three CRs in the MeVac IgG-Fc *C.m.* i.t. only group (Figure 2B).

Analysis of the relative tumor volume changes of individual mice (Figures 2C–2G) shows that for most of the mice experiencing CRs in the MeVac IgG-Fc *C.m.* i.t. and αmPD-1 i.p. combination group, a sharp increase in tumor volume occurred in the first 3 days following the MeVac IgG-Fc *C.m.* i.t. injections before a rapid decrease of tumor volume (Figure 2F).

To assess the safety of administering systemic versus MeVac-encoded PD-1 checkpoint blockade, we measured αmPD-1 levels in sera after treatment with αmPD-1 intravenously (i.v.), αmPD-1 i.p., or MeVac αmPD-1 i.t. (Figure S4). Sera were tested positive for αmPD-1 after systemic (i.v. or i.p.) dosing. In contrast, despite detecting MeVac mRNA within tumors, we did not detect αmPD-1 in mouse sera after treatment with MeVac αmPD-1. Having demonstrated comparable efficacy and potentially improved safety, we further pursued i.t. MeVac αmPD-1 as an approach for combination of measles virotherapy and PD-1/PD-L1 checkpoint blockade.

Therapeutic efficacy of MeVac αmPD-1 and MeVac αmPD-L1

Next we assessed therapeutic efficacy of the novel MeVac αmPD-1 vector compared with the previously developed MeVac αmPD-L1 in the subcutaneous MC38cea tumor model (Figures 3 and S5), as outlined in Figure 3A. MeVac IgG-Fc *C.m.* and MeVac IgG1-Fc were used as controls. Treatment with MeVac vectors significantly delayed tumor growth and prolonged survival of the animals in comparison with mock treatment (Figures 3B–3G and S5B–S5G).

When treatment was initiated on day 4 after tumor implantation (as in the experiment presented in Figure 2), four of ten mice in the MeVac IgG-Fc *C.m.*, MeVac IgG1-Fc, and MeVac αmPD-1 groups and five of ten mice in MeVac αmPD-L1 group experienced CRs (Figure 3).

In a second experiment, treatment was initiated on day 5 after tumor implantation (Figure S5A). In this case, there were no CRs in the MeVac IgG-Fc *C.m.* and MeVac IgG1-Fc control groups, while two of ten and three of ten mice had CRs in the MeVac αmPD-L1 and MeVac αmPD-1 groups, respectively (Figure S5B).

Analysis of the relative tumor volume changes of individual mice showed that in most animals in both experiments, there was an initial decrease in tumor volume following treatment with any of the MeVac variants (Figures 3C–3G and S5C–S5G). Afterward, in several animals this decrease in tumor volume continued and resulted in complete tumor remissions, while in others tumor growth resumed. In one experiment in the group receiving treatment with MeVac αmPD-L1, tumor growth was delayed longer in more animals than

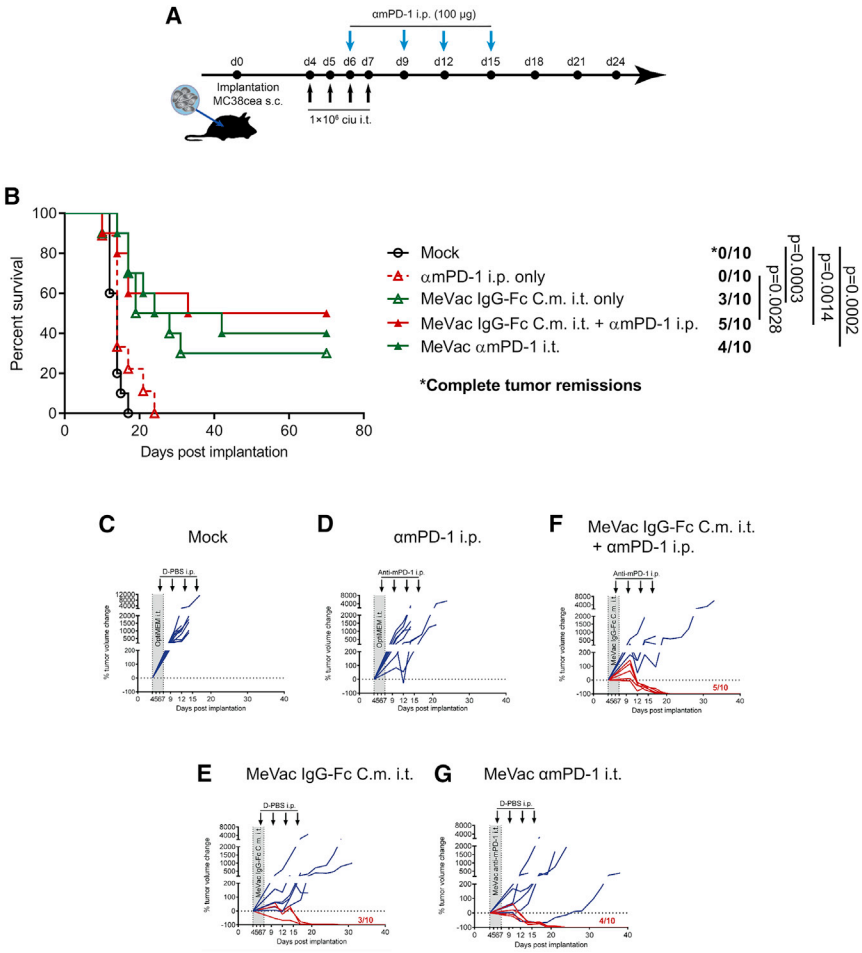

Figure 2. Therapeutic efficacy of intratumoral MeVac encoding αmPD-1 compared with combining intratumoral MeVac and systemic αmPD-1

(A) MC38cea cells were implanted subcutaneously into the right flanks of C57BL/6J mice. Treatment was initiated according to the depicted schedule when tumors reached an average volume of 55 mm^3. Animals received intratumoral (i.t.) injections with 1×10^6 cell infectious units of control vector MeVac IgG-Fc *C.m.* or MeVac αmPD-1 or i.t. injections of OptiMEM in control groups on 4 consecutive days. In the groups receiving systemic therapy with an antibody against murine PD-1 (αmPD-1), animals received intraperitoneal (i.p.) injections with 100 μg of J43 antibody on days 6, 9, 12, and 15 after tumor implantation. In the groups that did not receive systemic αmPD-1, animals received i.p. injections with PBS. Tumor volume was measured every third day. (B) Kaplan-Meier survival analysis with Mantel-Cox (log rank) test with Bonferroni correction for multiple comparisons. (C–G) Relative change in tumor volume in comparison with pre-treatment tumor volume of individual animals in the respective treatment groups. Tumor volume curves of mice with complete remission are highlighted in red.

in the groups receiving treatment with the other MeVac constructs (Figure 3E).

Tumor immune environment following MeVac αmPD-1 or MeVac αmPD-L1 therapy

We further aimed to analyze changes in the tumor immune environment following treatment with MeVac αmPD-1 or MeVac αmPD-L1. As in previous experiments with MeVac αmPD-L1,[24] we used the s.c. MC38cea tumor model and collected tumor samples for analysis 4 days after the last treatment (Figure 4A). First, we analyzed changes in the levels of seven different intratumoral cytokines. The results showed a trend toward increased IFN-γ and TNF-α levels in tumors following therapy with MeVac αmPD-L1 or MeVac αmPD-1 in comparison with mock treatment, while in the MeVac IgG1-Fc and MeVac IgG-Fc *C.m.* groups, the levels of these cytokines remained comparable with mock (Figures 4B and 4C). We did not detect any meaningful changes in the levels of interleukin (IL)-6, IL-2, IL-10, IL-17, and IL-4. Furthermore, we analyzed intratumoral T and NK cell populations following MeVac therapy by flow cytometry. The gating strategy is shown in Figure S6. We observed an increase in the intratumoral $CD8^+$ T cell population following treatment with all MeVac constructs. A trend toward a higher abundance of $CD8^+$ cells in tumors following treatment with MeVac αmPD-L1 compared with MeVac IgG1-Fc was observed (Figure 4D), but the same was not observed for MeVac αmPD-1 and the respective control vector (Figure 4E). Also, an increase in the abundance of intratumoral $CD4^+$ cells was observed following treatment with MeVac αmPD-L1 and MeVac IgG1-Fc in comparison with mock, with a trend toward a higher abundance of $CD4^+$ cells in the MeVac αmPD-L1 group (Figure 4F). No statistically significant differences in the $CD4^+$ cell population were observed in the experiment assessing MeVac αmPD-1 (Figure 4G). The NK cell population ($CD335^+$) was significantly reduced in the MeVac αmPD-L1 group in comparison with mock, while there were no differences among all the other analyzed groups (Figures S7A and S7B). We further determined expression of the early activation marker CD69 on the surface of intratumoral $CD8^+$, $CD4^+$, and NK cells following the different treatments. We observed significantly smaller $CD8^+CD69^+$ and $CD4^+CD69^+$ populations following treatment with MeVac αmPD-L1 and MeVac IgG1-Fc in comparison with the mock group (Figures 4H and 4J). A trend toward smaller $CD8^+CD69^+$ and $CD4^+CD69^+$ populations was also observed following treatment with MeVac αmPD-1 and MeVac IgG-Fc *C.m.* compared with the mock group, although the differences between the mock and MeVac IgG-Fc *C.m.* groups were not significant (Figures 4I and 4K). The $CD4^+CD69^+$ population was reduced in three tumors treated with MeVac αmPD-1, although no significant differences in comparison with mock and MeVac IgG-Fc *C.m.* treatment groups were observed when considering all tumor samples

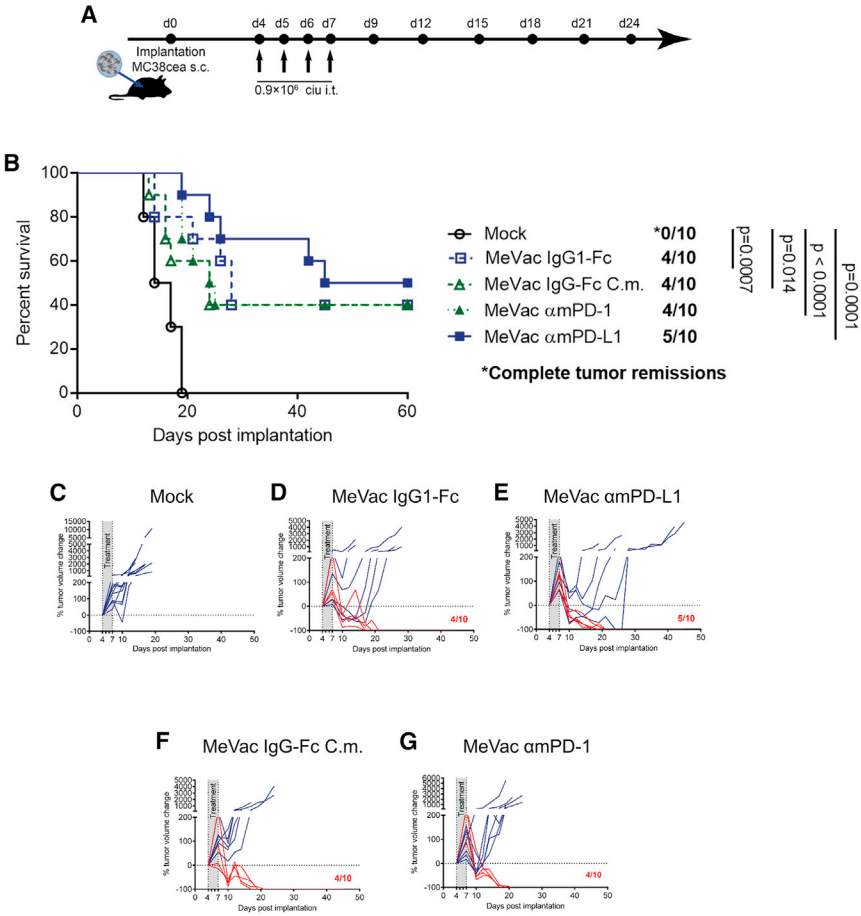

Figure 3. Therapeutic efficacy of MeVac αmPD-1 in comparison with MeVac αmPD-L1

(A) MC38cea cells were implanted subcutaneously into the right flanks of C57BL/6J mice. Treatment was initiated when the average tumor volume reached 45 mm^3. Animals received intratumoral (i.t.) injections with 0.9×10^6 cell infectious units of MeVac vectors encoding the respective transgenes on 4 consecutive days. Animals in the mock group received i.t. injections with OptiMEM. Tumor volume was measured every third day. (B) Kaplan-Meier survival analysis with Mantel-Cox (log rank) test with Bonferroni correction for multiple comparisons. (C–G) Relative change in tumor volume in comparison with pre-treatment tumor volume in individual animals of the respective treatment groups. Tumor volume curves of mice with complete remission are highlighted in red.

(Figure 4K). No significant changes in CD69 expression were observed in the $CD335^+$ NK cell population, although there was a trend toward a smaller $CD69^+$ population in the group receiving MeVac αmPD-1 (Figures S7C and S7D).

Tumor-specific immune memory following treatment with MeVac

We further assessed establishment of a long-term anti-tumor immune response in animals that experienced complete tumor remissions after treatment with MeVac vectors (experiments shown in Figures 3 and S5). To this end, MC38 cells were implanted s.c. in the flank contralateral to the primary tumor, and regrowth of secondary tumors was monitored. Tumor regrowth after implantation was observed in five of six naive animals. In contrast, all of the animals that previously experienced complete tumor remissions rejected secondary tumor engraftment in MeVac IgG1-Fc, MeVac αmPD-1, and MeVac αmPD-L1 groups, and three of four animals rejected tumor engraftment in the MeVac IgG-Fc *C.m.* group (Figure 5A). These results suggest establishment of long-term anti-tumor immunity against MC38 after MeVac therapy. To further examine the specificity of the observed anti-tumor effect, IFN-γ production of splenocytes from the same animals was assessed following stimulation with MC38 cells *in vitro*. The results revealed higher IFN-γ production by splenocytes isolated from the animals in the MeVac αmPD-1 and MeVac αmPD-L1 groups in comparison with naive animals and animals from MeVac IgG Fc *C.m.* and MeVac IgG1-Fc control groups (Figure 5B), suggesting a more robust anti-tumor immune memory response.

Memory T cell populations following MeVac αmPD-1 therapy

Following the observation of increased IFN-γ recall response after MeVac αmPD-1 and MeVac αmPD-L1 treatment, we further investigated the impact of MeVac αmPD-1 therapy on the memory T cell population. We analyzed expression of the markers CD44 and CD62L on $CD8^+$ and $CD4^+$ T cells to investigate changes in the functional subsets of memory T cells in tumors and in tumor-draining lymph nodes (TDLNs) 4 days after the last treatment by flow cytometry. The gating strategy is shown in Figure S8.

In tumors we observed a significantly higher ratio of effector memory (EM) ($CD44^{Hi}CD62L^-$) to central memory (CM) T cells ($CD44^{Hi}CD62L^+$) among both $CD8^+$ and $CD4^+$ T cell populations following treatment with MeVac IgG-Fc *C.m.* and MeVac αmPD-1 in comparison with mock (Figures 5C and 5D). A trend toward a larger intratumoral EM/CM ratio of $CD4^+$ cells in comparison with the MeVac IgG-Fc *C.m.* group was observed in the MeVac αmPD-1 group, with considerable variation among individual mice.

In TDLNs there was no significant difference in the ratio of EM to CM T cells between treatment groups (Figures 5E and 5F). However, there was a relative decrease in CM and relative increase in EM T cells after treatment with MeVac αmPD-1 (not shown).

MeVac encoding pembrolizumab, nivolumab, or atezolizumab

In addition to MeVac encoding the anti-PD-L1 antibody atezolizumab,[24] we generated MeVac vectors encoding the clinically approved

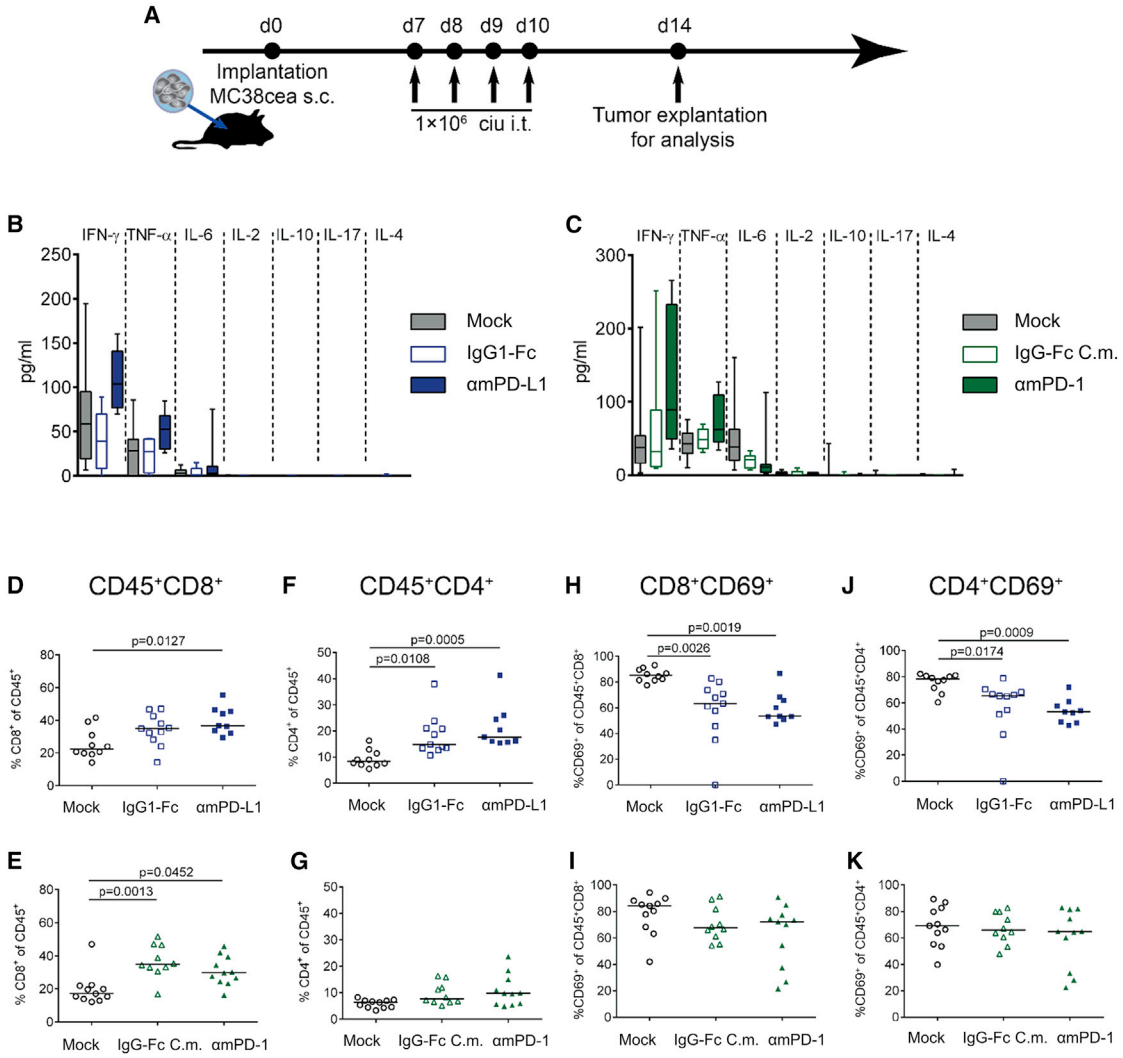

Figure 4. Immunomodulatory effects of MeVac αmPD-1 and MeVac αmPD-L1

(A) MC38cea cells were implanted subcutaneously into the right flanks of C57BL/6J mice. Treatment was initiated when the average tumor volume reached 100 mm^3 (n = 9–12 per group). Animals received intratumoral injections with 1 × 10^6 cell infectious units of MeVac vectors encoding the respective transgenes on four consecutive days. Animals in the mock group received i.t. injections of OptiMEM. Animals were sacrificed and tumors were explanted 4 days after the last treatment. (B and C) Protein extraction was performed from a sample of each of the explanted tumors, and cytokine bead array was performed to measure intratumoral concentrations of seven different cytokines. Box-and-whisker plots with whiskers depicting minimal and maximal detected concentrations as well as median in each group are shown. (D–K) Samples from each of the explanted tumors were prepared for flow cytometry analysis. The percentages of cytotoxic T cells ($CD8^+$), T helper cells ($CD4^+$), activated cytotoxic ($CD8^+$ $CD69^+$), and helper ($CD4^+$ $CD69^+$) T cells among leukocytes ($CD45^+$) were determined. Dots representing individual tumors and bars representing the median in the group are shown. Data were analyzed using one-way ANOVA with Dunn's multiple-comparisons post hoc test.

anti-PD-1 antibodies pembrolizumab and nivolumab. In analogy to a previously described adeno-associated viral (AAV) vector,[55] transgene cassettes constituting a Kozak sequence, Igκ leader, and the respective antibody heavy and light chains separated by an F2A linker were inserted downstream of the MeVac H gene (Figure 6A). MeVac encoding human IgG4 Fc only was generated as a control vector.

Replication kinetics of the novel vectors were analyzed in Vero cells and the human colorectal adenocarcinoma cell lines Colo 205 and HT-29 (Figure 6B). ELISA of infected cell supernatants revealed secretion of pembrolizumab and nivolumab after inoculation with the respective recombinant MeVac vectors (Figure 6C). Interestingly, nivolumab appeared to be expressed at higher levels. Binding of pembrolizumab and nivolumab secreted from cells infected with the respective vectors to PD-1^+ human immune cells was confirmed using flow cytometry (Figure 6D). As demonstrated previously, atezolizumab secreted from cells infected with MeVac encoding this anti-PD-L1 antibody bound to PD-$L1^+$ human colorectal cancer cells (Figure S9).

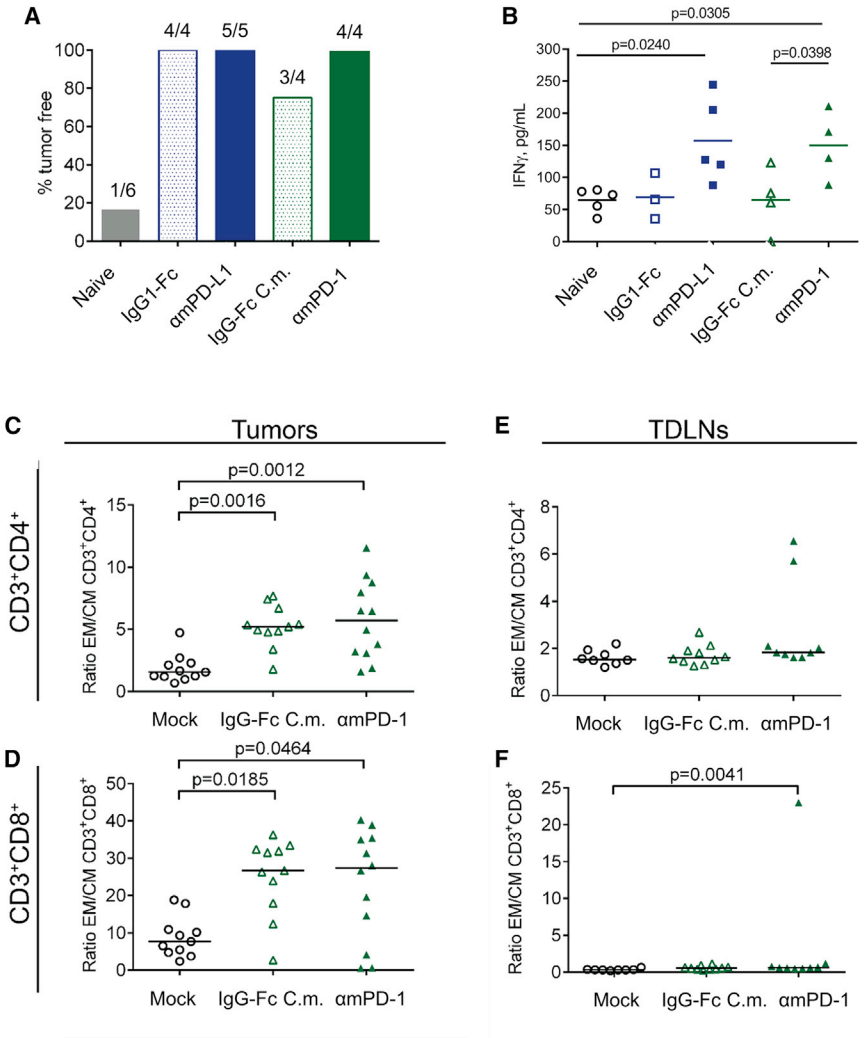

Figure 5. Memory T cell populations in tumors and tumor-draining lymph nodes following therapy with MeVac αmPD-1

(A) Animals that experienced complete tumor remissions after treatment with the indicated MeVac variants (as shown in Figure 3) were rechallenged with s.c. injection of MC38 cells in the left flanks ~60 days after initial tumor implantation. Age-matched naive mice were used as controls. Tumor growth was monitored every third day. Tumor rejection rates in the respective group are shown. (B) Spleens were explanted from animals used in the re-challenge experiment and splenocytes were stimulated with MC38 cells for 48 h *in vitro*. IFN-γ concentration in the supernatants was measured using ELISA. Dots representing individual animals and bars depicting mean value in the group are shown. Data were analyzed using one-way ANOVA with Tukey's multiple-comparisons test. (C–F) MC38cea tumor cells were implanted into the right flanks of C57BL/6J mice. When the average tumor volume reached 100 mm^3, animals were assigned to treatment groups (n = 10–12 per group) and received intratumoral (i.t.) injections with 1×10^6 ciu/mL of MeVac αmPD-1 or MeVac IgG-Fc *C.m.* Animals in the mock group received i.t. injections of OptiMEM. Four days after the last treatment, animals were sacrificed and flow cytometric analyses of tumors and tumor-draining lymph nodes (TLDNs) were performed. Markers CD44 and CD62L were used to discriminate the effector memory (EM) T cells ($CD44^{Hi}CD62L^{-}$) and central memory (CM) T cells ($CD44^{Hi}CD62L^{+}$). Ratio of EM to CM T cells among $CD3^{+}CD4^{+}$ or $CD3^{+}CD8^{+}$ T cells is shown. Dots representing the individual animals with median in the group are depicted. Data were analyzed using one-way ANOVA with Dunn's multiple-comparisons post hoc test.

To test whether MeVac-encoded anti-human PD-1 antibodies can re-invigorate T cells, we stimulated peripheral blood mononuclear cells (PBMCs) with varying concentrations of *Staphylococcus* enterotoxin B (SEB) and added supernatants from cells infected with MeVac encoding pembrolizumab, nivolumab, or IgG4. Supernatants from cells infected with MeVac encoding pembrolizumab or nivolumab elicited increased levels of interleukin-2 secretion, indicating T cell activation (Figure 6E). Interestingly, MeVac pembrolizumab samples elicited higher IL-2 levels after 40 h of incubation, while MeVac nivolumab samples elicited higher IL-2 levels after 70 h of incubation.

DISCUSSION

Immune checkpoint blockade targeting the PD-1/PD-L1 axis is a pillar of many successful treatment strategies. Various combination treatments including anti-PD-1 and anti-PD-L1 antibodies are currently investigated in clinical trials.[31] Oncolytic viruses are appealing combination therapeutics for cancer immunotherapy that induce immunogenic tumor cell death and promote tumor-specific T cell responses.[32,33] Supporting this notion, combination of the FDA-approved oncolytic herpes virus talimogene laherparepvec with pembrolizumab has achieved remarkable response rates in advanced melanoma.[15] Instead of combination treatment, encoding checkpoint blocking antibodies within an oncotropic vector has the benefit of increasing local concentrations at the tumor site while decreasing systemic exposure, thereby optimizing the therapeutic index. This concept of encoding PD-1/PD-L1 antibodies has been adopted to various oncolytic platforms, including adenovirus[34] and herpes virus.[35] We have previously described oncolytic measles viruses encoding antibodies against PD-L1[12] and tested their efficacy in the MC38cea model.[24] Here, we report the generation and assessment of oncolytic measles vaccine vectors encoding antibodies against mouse and human PD-1.

Overall, we observed a modest benefit of combining PD-1/PD-L1 checkpoint blockade with oncolytic measles virus in the MC38cea model, although this tumor displays features generally associated with response to PD-1/PD-L1 checkpoint blockade: MC38cea has a high mutational load[36] and shows PD-L1 expression, which is further upregulated upon MeVac treatment (Figure S1).

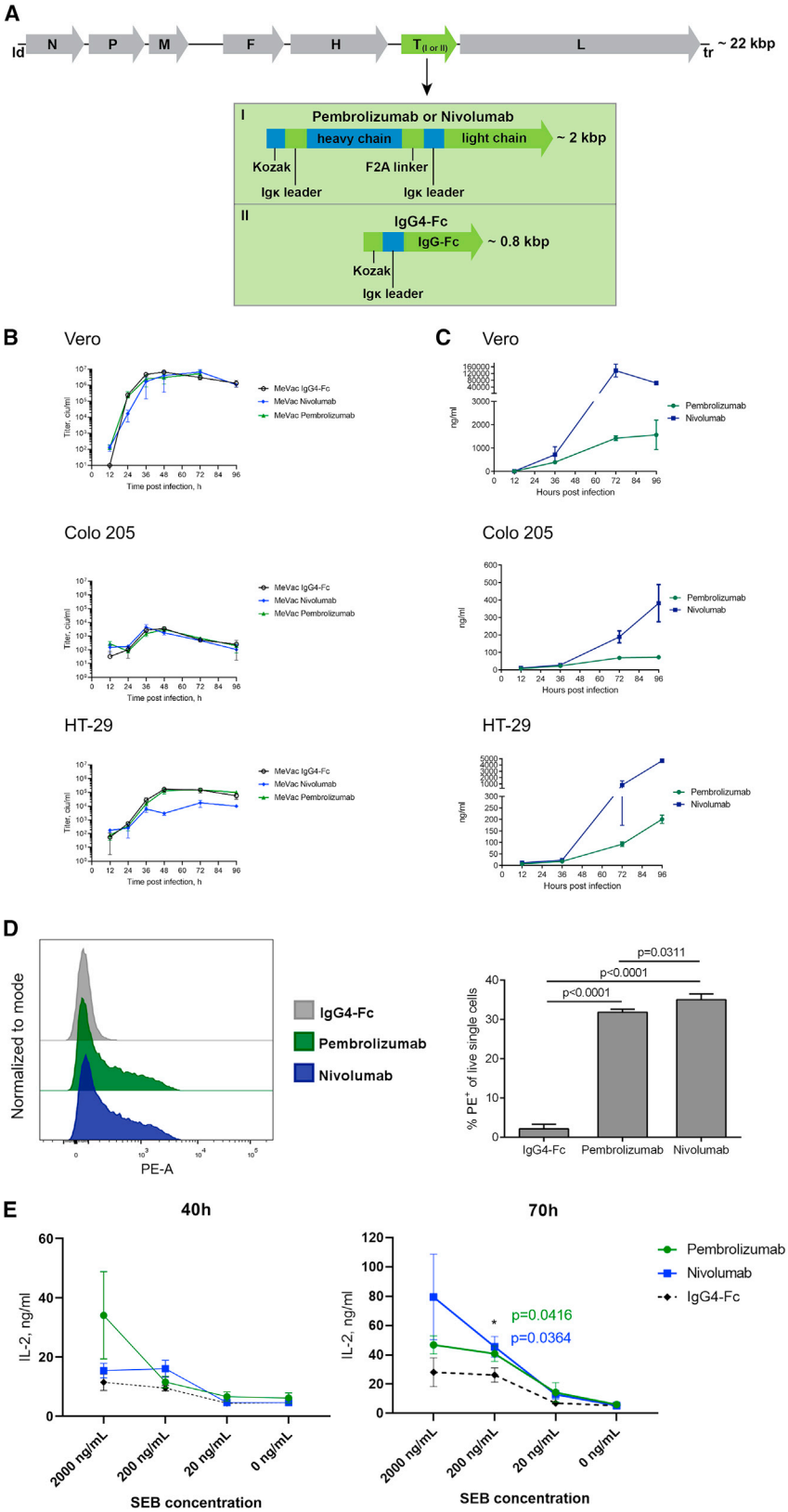

Figure 6. MeVac vectors encoding pembrolizumab and nivolumab

(A) Vector design. Schematic of MeVac vectors encoding the respective transgenes (T). Transgene cassettes include a Kozak sequence, mouse immunoglobulin κ secretion signal, and (I) the respective light and heavy chains of pembrolizumab or nivolumab connected by an F2A linker or (II) the human IgG4 Fc region. (B and C) Replication kinetics and transgene expression. Simian Vero as well as human colorectal carcinoma Colo 205 and HT-29 cells were infected with indicated MeVac variants at MOI = 3. (B) Viral progeny were determined at designated time points by serial dilution titration assay. Mean values of quadruplicates and SDs are shown. (C) Concentrations of nivolumab and pembrolizumab in cell culture supernatants were determined using ELISA. (D) Binding of MeVac-encoded pembrolizumab or nivolumab to PD-1^{+} human immune cells. Peripheral blood mononuclear cells (PBMCs) from healthy donors were stimulated with PMA and ionomycin, which induces PD-1 expression. Stimulated PBMCs were incubated with supernatants from Vero cells infected with MeVac encoding IgG4, pembrolizumab, or nivolumab and stained with a PE-labeled antibody specific for human IgG-Fc. Data from three independent experiments were analyzed using one-way ANOVA with Tukey's multiple-comparisons test. (E) Functional assay for pembrolizumab and nivolumab. Human PBMCs were stimulated with SEB and incubated with supernatants from Vero cells infected with MeVac encoding pembrolizumab, nivolumab, or IgG4-Fc. After 40 and 70 h, IL-2 concentration in PBMC culture supernatants was determined using ELISA. Results were analyzed using two-way ANOVA with Tukey's multiple-comparisons test.

However, murine tumors show limited permissiveness for measles virus, thus limiting the levels of antibody expression (Figures 1B, 1C, and S2B). Moreover, different PD-1 antibody clones may yield different outcomes. There is an ongoing debate regarding which PD-1 clone and Fc fragment is optimal to block inhibitory signals without depleting tumor-reactive effectors cells.[37,38]

In this regard, pre-clinical mouse models with xenogeneic antibodies do not recapitulate clinically applied anti-PD-1/PD-L1, limiting the transferability to clinical treatment settings.[39] In contrast to murine tumors, we observed high levels of pembrolizumab and nivolumab secretion from human cancer cells infected with the respective MeVac vectors (Figure 6). Thus, we would expect stronger effects against human tumors.

We observed no significant differences in efficacy of the MeVac-encoded anti-PD-1 compared with the combination of MeVac with systemic anti-PD-1 (Figure 2B). This is in line with our previous findings in a different murine tumor model (B16 melanoma), in which an oncolytic measles vaccine virus (Edmonston B-derived) encoding anti-PD-L1 showed similar efficacy as the combination of virus and systemic PD-L1 antibody.[12] PD-1 blockade has been found to also act in tumor-draining lymph nodes.[40,41] In line with previous studies with C57BL/6 mice,[42] we did not detect MeVac mRNA in TDLN (data not shown). However, as the TDLN have been shown to play an essential role in response to PD-1/PD-L1 checkpoint blockade in the MC38 model,[40] we assume that effects of intratumorally administered MeVac vectors may extend to the TDLNs via recirculating immune cells.

Analyses of the tumor immune environment revealed subtle changes upon MeVac-mediated PD-1/PD-L1 checkpoint blockade. Of note, oncolytic measles virotherapy alone (i.e., treatment with MeVac IgG1-Fc) already leads to activation of innate and adaptive immunity in the MC38cea model, as shown by previously published gene expression profiling.[43] Tumors that are less responsive to MeVac alone may show more added benefit of combination with PD-1/PD-L1 checkpoint blockade. This notion is supported by data from other models of measles virus oncolysis.[12,43,44] In tumor samples, we observed an increase in inflammatory effector cytokines after treatment with MeVac, which was enhanced with vectors encoding PD-1/PD-L1 antibodies (Figures 4B and 4C). In individual mice, an initial increase in tumor volume was observed before tumor regression. This may be attributable to acute intratumoral inflammation upon virotherapy or perhaps resemble the clinical phenomenon of pseudoprogression during cancer immunotherapies,[45] although kinetics differ from clinical settings in this rapidly progressing transplantable mouse tumor model.

We found slight changes in the intratumoral and TDLN T cell compartments upon MeVac αPD-1/PD-L1 treatment. Although there was a trend toward increased overall abundance of both intratumoral $CD8^+$ and $CD4^+$ T cells, we observed a decrease in T cells expressing the early activation marker CD69 (Figures 4D–4K). This may be explained by a shift toward a T cell effector memory phenotype (Figures 5C–5F). As NK cell activation has been implicated in PD-1/PD-L1 checkpoint blockade,[46] we also analyzed this subset of tumor-infiltrating immune cells but found no significant changes in their abundance or activation status. Longitudinal analyses including in-depth phenotyping across multiple time points could provide insights into the dynamics of the tumor immune environment. These results could pinpoint effector mechanisms involved in response and also possible resistance factors such as oncogenic signaling, myeloid-derived suppressor cells, or alternative immune checkpoints limiting response to PD-1/PD-L1 checkpoint blockade.[47] These factors could be targeted by alterations of the treatment regimen, including additional modifications of MeVac vectors. Toward this end, oncolytic measles vaccine viruses provide a flexible platform to develop safe immunotherapeutic vectors.[18] Several immunotherapeutic strategies have been implemented using this platform that could be adopted in this context. In case insufficient T cell effector functions are identified as limiting MeVac αPD-1/PD-L1 therapy, interleukin-12 could be incorporated.[24] If tumor cell recognition is deemed insufficient, bispecific T cell engagers (BiTEs) could be encoded in the vector. Our previous results suggested benefits from combining oncolytic measles viruses encoding BiTEs with immune checkpoint blockade.[48] Other resistance mechanisms such as pro-tumorigenic signaling or myeloid-derived suppressor cells[47,49,50] could also be addressed using advanced oncolytic vectors.

Importantly, despite limited effects of MeVac-encoded αmPD-1 and αmPD-L1 on the immediate treatment response, we did detect protective immune memory and an enhanced tumor-specific memory recall response after treatment with MeVac αmPD-1 and MeVac αmPD-L1.

The vectors we developed, which encode the clinically approved PD-1 blocking antibodies pembrolizumab and nivolumab, could provide benefits in this regard. We therefore envision this therapeutic approach in a setting with minimal residual disease. In such a scenario, MeVac encoding anti-PD-1/PD-L1 could be used to lyse remaining tumor cells and induce anti-tumor immunity via oncolytic vaccination effects, which are then consolidated into long-term protective anti-tumor memory responses.

MATERIALS AND METHODS

Cell lines

The African green monkey kidney cell line Vero was obtained from the American Type Culture Collection (CCL-81). The Vero-αHis cell line stably expressing a single chain antibody against His_6[51] tag was a gift from S. J. Russell (Mayo Clinic, Rochester, MN). The murine colorectal adenocarcinoma cell line MC38 and the MC38 cell line transduced for stable expression of a human CEA (MC38cea[52]) were obtained from R. Cattaneo (Mayo Clinic). The cell line Colo 205 (CCL-222) was obtained from A. Jassowicz (Deutsches Krebsforschungszentrum [DKFZ], Heidelberg, Germany). The cell line HT-29 (HTB-38) was obtained from C. Plass (DKFZ). B16-CD46 and MC38-CD46 cells stably expressing human CD46 were generated

as described previously.[48] Vero, Vero-αHis, MC38, MC38-CD46, and MC38cea cells were cultivated in Dulbecco's modified Eagle's medium (DMEM) (3196604; Life Technologies) supplemented with 10% fetal calf serum (FCS) (FB-1000/500 [Biosera, Nuaillé, France] and FBS Good [Pan-Biotech, Aidenbach, Germany]). B16-CD46, Colo 205, and HT-29 cell lines were maintained in Roswell Park Memorial Institute (RPMI) 1640 medium (61870044; Life Technologies) with 10% FCS. The CTL-ova cell line has been described previously.[53] CTL-ova cells were provided by S. Eichmüller and W. Osen (DKFZ) and cultivated in α-MEM medium (Sigma-Aldrich, Taufkirchen, Germany) supplemented with 10% FCS, 4 mM L-glutamine, 100 U/mL penicillin, 100 μg/mL streptomycin, and 10 μM β-mercaptoethanol (all from Thermo Fisher Scientific, Schwerte, Germany) and restimulated as described before.[54] All cell lines were cultivated at 37°C in a humidified atmosphere with 5% CO_2. Routine tests for mycoplasma contamination were performed.

Cloning and generation of recombinant MeVac

MeVac eGFP, cloning of MeVac encoding an antibody against murine/human PD-L1 (MeVac αmPD-L1; antibody sequence corresponds to clinically used atezolizumab), and MeVac encoding the antibody constant region IgG1-Fc (MeVac IgG1-Fc) have been described previously.[24] The cassette encoding an antibody against murine PD-1 (αmPD-1) was designed in analogy to the existing anti-murine/human-PD-L1 construct. In contrast to the αPD-L1 (atezolizumab) cassette, in which the constant region corresponds to human IgG1-Fc, in the novel αmPD-1 construct we used hamster (*Cricetulus migratorius*) IgG-Fc (IgG-Fc *C.m.*). The αmPD-1 corresponds to clone J43, which is of *C.m.* origin. The αmPD-1 cassette consists of the following elements: a Kozak sequence, the Igκ leader sequence, an HA tag, the variable light chain sequence of J43, a $(Gly_4Ser)_3$ linker, the variable heavy-chain sequence of J43, the Fc region of the antibody, and a myc tag. To comply with the "rule of six,"[55] a TA spacer was inserted at the 3′ end of the construct. GENEius codon optimization for expression in murine cells was performed to obtain the final sequence (Eurofins MWG Operon, Ebersberg, Germany). The cassette encoding IgG-Fc *C.m.* was designed similarly and consisted of a Kozak sequence, the Igκ leader sequence, an HA tag, the IgG-Fc *C.m.* sequence, and a myc tag. Both αmPD-1 and IgG-Fc *C.m.* cassettes were flanked by MluI and AscI restriction sites. After restriction digest with MluI and AscI, the αmPD-1 (1,914 bp) or the IgG-Fc *C.m.* (1,182 bp) cassette was inserted into the additional transcription unit (ATU) downstream of the MeVac H gene via the unique MauBI site, yielding MeVac αmPD-1 or MeVac IgG-Fc *C.m.* In MeVac αmPD-L1, MeVac IgG1-Fc, MeVac αmPD-1, and MeVac IgG-Fc *C.m.* the MeVac H protein was fully retargeted to human CEA as described previously[28] to allow infection of murine MC38cea cells.

The cassette encoding the nivolumab construct has been described previously.[30] For insertion into the MeVac genome, the nivolumab cassette was generated by PCR using the existing construct as a template. The cassette encoding pembrolizumab was designed in analogy to the nivolumab construct. Both nivolumab and pembrolizumab constructs consist of the following elements: a Kozak sequence, an Igκ leader sequence, and the open reading frame (ORF) of the variable heavy chain of the antibody followed by an F2A linker, an Igκ leader sequence, and an ORF for the variable light chain of the antibody ending with an additional stop codon and a TA spacer to comply with the "rule of six" after insertion into the MeVac genome. The sequence of the novel pembrolizumab construct was optimized for *Homo sapiens* codon use with the GENEius codon optimization tool, and the final construct was obtained by gene synthesis (Eurofins MWG Operon). The IgG4-Fc construct consisting of a Kozak sequence, the Igκ leader sequence, the IgG4-Fc sequence, and a TA spacer was generated by PCR using the nivolumab construct as a template. All final constructs were flanked by MluI and AscI restriction sites. After restriction digest, the MluI-AscI fragment containing the pembrolizumab (2,208 bp), nivolumab (2,172 bp), or IgG4-Fc (768 bp) cassette was inserted into an ATU downstream of the MeVac H gene via the unique MauBI site, yielding MeVac pembrolizumab, MeVac nivolumab, or MeVac IgG4-Fc.

Infectious viruses were obtained from the cDNA constructs using the reverse genetics system originally described by Radecke et al.,[56] which was later adapted for RNA polymerase II.[57] The detailed method to obtain viral particles from the generated antigenomic constructs of recombinant MeVac vectors has been described previously.[58]

MeVac propagation, titration, and *in vitro* infection experiments

Procedures for propagation and titration of recombinant measles vectors have been described in detail previously.[58] In brief, for propagation, Vero or Vero-αHis cells were inoculated with MeVac at a multiplicity of infection (MOI) of 0.03 in OptiMEM. After 2–3 h the inoculum was removed, DMEM + 10% FCS was added onto the cell layer, and cultivation was continued. When syncytia had spread across the entire cell layer, the cells were scraped, harvested, and snap-frozen in liquid nitrogen. The collected samples were thawed and centrifuged at 2,500 × *g* for 5 min to remove cell debris, and the cleared supernatants were aliquoted and stored at −80°C. Viral titers were determined by performing 1:10 serial dilution titration assays on Vero or Vero-αHis cells in 96-well flat-bottom plates in octuplicates per dilution. The concentration of viral cell infectious units per milliliter (ciu/mL) was calculated by multiplying the average count of single syncytia per well per dilution 48 or 72 h post-infection with the respective dilution factor.

For *in vitro* infection experiments, the respective cells were seeded 1 day before inoculation. Inoculation with MeVac at the indicated MOI was performed in OptiMEM. The inoculum was removed after 2–3 h of cultivation, the cell line-specific medium was added, and cultivation was continued. Cell viability assays were performed with the Colorimetric Cell Viability Kit III (2,3-bis-[2-methoxy-4-nitro-5-sulfophenyl]-2H-tetrazolium-5-carboxanilide [XTT]) (PromoKine, Heidelberg, Germany).

Western blot for αmPD-1 and IgG-Fc *C.m.*

Vero-αHis and MC38cea cells were seeded in 10 cm tissue culture plates and infected with MeVac αmPD-1 or MeVac IgG-Fc *C.m.* at MOI = 3. Supernatants from the infected plates (volume ∼ 12 mL) were collected at 0, 10, 24, 48, 72, and 96 h post-infection (from one plate per time point), snap-frozen in liquid N_2, and stored at −80°C until further processing. The samples were thawed in a water bath at 37°C and sterile filtrated through a 0.2 μm filter. Afterward, immunoprecipitation was performed using Sepharose A beads (Biocat, Heidelberg, Germany). Sepharose A beads were washed three times with D-PBS (20 μL beads per sample) and after resuspension in D-PBS, beads were added to each sample. The samples were incubated for 1 h with rotation at room temperature (RT). After incubation, the beads were spun down for 3 min at 100 × *g*, washed twice with D-PBS, and resuspended in D-PBS. For denaturation, samples were diluted with 1× Laemmli buffer and incubated for 5 min at 95°C. Sodium dodecyl sulfate-polyacrylamide gel electrophoresis (SDS-PAGE) and immunoblot analysis were performed as described in detail previously[12]: SDS-PAGE was performed using a 12% polyacrylamide gel (Mini-PROTEAN TGX; BioRad, Munich, Germany) at 200 V for 35 min, followed by a sample transfer onto a polyvinylidene fluoride membrane (Immobilon; Merck Millipore, Schwalbach, Germany) using a wet-blot chamber (Mini-PROTEAN Tetra Cell; BioRad) in Novex TrisGlycine Transfer Buffer (Invitrogen). The membrane was blocked for 30 min at room temperature using 5% skim milk in a TBS-T buffer. Afterward, the membrane was incubated for 2 h at RT with the primary antibody mouse anti-HA (clone HA-7) (Sigma-Aldrich) diluted 1:10,000 in 5% skim milk in TBS-T. Subsequently, the membrane was washed three times with TBS-T for 5 min and incubated for 2 h at RT with the secondary antibody anti-mouse IgG-HRP (Bethyl, Montgomery, TX) diluted at 1:2,000 in 5% skim milk in TBS-T. After washing three times with TBS-T, SuperSignal West PICO Chemiluminescent Substrate (Thermo Fisher, Schwerte, Germany) was added onto the membrane, and images were acquired using the ChemiDOC XRS Imaging System (BioRad). The relative band intensity in comparison with 0 h post-infection (intensity = 1) in the images was analyzed using ImageJ2.[59]

Flow cytometry assay for binding of MeVac-encoded antibodies to target cells

Vero-αHis or Vero cells were seeded in 15 cm tissue culture plates and infected with MeVac αmPD-1, MeVac IgG-Fc *C.m.*, MeVac αmPD-L1 or MeVac IgG1-Fc (Vero-αHis) or MeVac pembrolizumab, MeVac nivolumab, or MeVac IgG4-Fc (Vero) at MOI = 0.03. When syncytia had spread across the entire cell layer (∼39 h post-infection for Vero-αHis infections and ∼48 h post-infection for Vero infections), the entire supernatant from each plate was collected, snap-frozen in liquid N_2, and stored at −80°C until further use. The samples were thawed in a water bath at 37°C and sterile filtrated through a 0.2 μm filter. The supernatant from each plate (∼15 mL) was subjected to concentration using Amicon Ultra-15 10K Centrifugal Filter Device (Merck Millipore, Darmstadt, Germany) for 20 min at 4,000 × *g* at RT. Then the filtrate that passed through the membrane was removed and 13 mL D-PBS was added to the concentrate, and centrifugation for 20 min at 4,000 × *g* at RT was repeated. The resulting concentrate (∼300 μL) was collected for further use. To test binding of anti-PD-L1, 1×10^6 MC38cea cells were incubated with the supernatant samples containing αmPD-L1 or IgG1-Fc. To test binding of PD-1 targeting antibodies, 2×10^6 murine CTL-ova cells were incubated with the concentrated samples containing αmPD1 or IgG-Fc *C.m.*, and 2×10^6 human PBMCs (activated for 24 h with 5 nM PMA and 500 nM ionomycin) were added to samples containing pembrolizumab, nivolumab, or IgG4-Fc. The cells were incubated with the concentrates for 20 min at RT. The cells were then spun down for 5 min at 300 × *g* and resuspended in 100 μL D-PBS per sample. MC38cea and CTL-ova cells were stained with 10 μL PE anti-HA tag (Clone GG8-1F3.3.1) (Miltenyi Biotech, Bergisch-Gladbach, Germany). CTL-ova cells were also stained with 1 μL APC Rat Anti-Mouse CD8a (clone 53-6.7) (BD Biosciences, Heidelberg, Germany) per sample, human cells were stained with 5 μL anti-human IgG-Fc-PE (BioLegend, London, United Kingdom) per sample and incubated for 30 min at RT in the dark. For the experiment with murine cells, as a positive control, 1×10^6 CTL-ova in 100 μL were stained with 1 μL PE anti-mouse CD279 (PD-1) (clone RMP1-30) (BioLegend) and 1 μL APC Rat Anti-Mouse CD8a (clone 53-6.7) (BD Biosciences) and incubated for 30 min at RT in the dark. Afterward, 1 mL D-PBS was added to each stained sample and centrifuged at 300 × *g* for 5 min at RT. Each cell pellet was resuspended in 500 μL D-PBS with 0.2 μg 4′,6-diamidino-2-phenylindole (DAPI). Single stain and isotype controls were prepared using CTL-ova cells or freshly isolated human PBMCs in parallel to the samples and used for compensation and gating. The samples and controls were acquired on a BD FACS LSRII with FACSDiva software (version 8.0.1) and analyzed using FlowJo version 10.0.7r2 (Tree Star).

Competitive binding assays for anti-PD-1 and anti-PD-L1

Splenocytes from a 7-week-old C57BL/6 female mouse were cultured at 37°C and 5% CO_2 in non-treated six-well plates at 4×10^6 cells per well in 2 mL RPMI-GlutaMAX supplemented with 10% FCS, 50 μM 2-mercaptoethanol (Thermo Fisher Scientific), 1% penicillin/streptomycin (Thermo Fisher Scientific), 10 ng/mL PMA (Sigma-Aldrich), and 500 ng/mL ionomycin (Cayman Chemical, Ann Arbor, MI). After 72 h, the cells were harvested and incubated for 30 min at 4°C with 10 μL cell lysate from Vero-αHis cells infected with MeVac αmPD-1 and 10 μL of 5-fold dilutions of a commercial αmPD-1 antibody (stock concentration of 1 mg/mL, clone J43; Thermo Fisher Scientific) as competitor. Cell lysate from Vero-αHis cells infected with MeVac IgG-Fc *C.m.* was used as negative control.

MC38-CD46 cells and Colo 205 cells were seeded in six-well plates at 3×10^5 cells per well and infected 24 h afterward with MeVac at MOI = 3 and MeVac eGFP at MOI = 0.03, respectively. 48h after infection, the cells were harvested and incubated for 30 min at 4°C with 10 μL cell lysate from Vero-αHis cells infected with MeVac αmPD-L1 and 10 μL of 5-fold dilutions of commercial atezolizumab (stock concentration of 3.2 ng/mL; Heidelberg University Hospital Pharmacy, Heidelberg, Germany) as a competitor. Cell lysate from Vero-αHis cells infected with MeVac IgG1-Fc was used as negative control.

Mouse splenocytes, MC38-CD46 cells, and Colo 205 cells incubated with the corresponding cell lysates were stained with a PE anti-HA tag antibody (clone GG8-1F3.3.1; Miltenyi Biotech) at a 1:50 dilution for 30 min at 4°C in the dark. DAPI (Sigma-Aldrich) was used as a viability dye. The samples and controls were acquired on a BD FACSCanto II cytometer (BD). Data were analyzed using the BD FACSDiva software and FlowJo software.

Animal experiments

All experimental procedures with animals were approved by the regional council (Regierungspräsidium Karlsruhe, protocols G-192/15 and G-58/17) and performed in compliance with the German Animal Protection Law and institutional guidelines. Six- to eight-week-old female C57BL/6J mice were acquired from Harlan Laboratories (Rossdorf, Germany). Mice were housed in groups of five in individually ventilated cages at the Center for Preclinical Research of the German Cancer Research Center.

MC38cea cells (1×10^6) were subcutaneously implanted into the right flank of the animals in 100 μL total volume of D-PBS. When the average tumor volume reached approximately 50 mm^3 (for survival experiments) or 100 mm^3 (for analysis of tumor immune environment), the treatment was started according to the schedule of the respective experiment. For virus treatment, animals received intratumoral injections with 0.9×10^6 or 1.0×10^6 ciu of the respective MeVac construct in 100 μL. In the control groups of virus treatment, animals received i.t. injections with 100 μL of OptiMEM. For antibody treatment, animals received intraperitoneal injections with 100 μg of anti-mouse PD-1 (clone J43) antibody in 200 μL total volume. In control groups for antibody treatment, animals received i.p. injections with 200 μL D-PBS. Tumor growth was monitored by measuring the largest and smallest diameters of tumors every third day using a digital caliper. Tumor volume was calculated by using the formula largest diameter × smallest diameter^2 × 0.5.

In survival experiments animals were sacrificed when the tumor volume exceeded 1,000 mm^3, the largest tumor diameter exceeded 15 mm, tumor ulceration occurred, or the animals were moribund. In the experiments for tumor immune environment analysis, the animals were sacrificed at the pre-defined time point of analysis. For tumor rechallenge experiments, 1×10^5 MC38 cells were implanted into the left flank of the mice and tumor development was monitored every third day.

Cytokine bead array of tumor samples

Protein isolation from MC38cea tumor samples was performed as described previously.[60] In brief, freshly collected tumor samples were transferred into empty 1.5 mL tubes, snap-frozen in liquid N_2, and stored at −80°C until processing. Samples were thawed on ice, minced using a scalpel, and homogenized using an Eppendorf-fitting pestle in lysis buffer consisting of 10 mM Tris-HCl (pH 8.0), 150 mM NaCl, 10% glycerol, 5 mM EDTA, 1% NP-40, and one cOmplete Mini, EDTA-free Protease Inhibitor Cocktail Tablet (Sigma-Aldrich). The obtained lysates were incubated for 1 h at 4°C with rotation. The samples were then sonicated at an intermittent (0.5 min) on and off sonication regimen for 7 min (high intensity) using a Diagenode Bioruptor R Standard with a cooling water pump (Diagenode, Seraing, Belgium). The lysates were cleared by centrifugation at 13,000 × *g* for 15 min, and supernatants were collected and stored at −80°C until analysis. Cytokine concentrations were measured using the Mouse Th1/Th2/Th17 Cytokine Bead Array Kit (BD Biosciences) according to the instructions of the manufacturer.

For detection of virus-derived mRNA, tumor samples were collected in RNAlater (Thermo Fisher Scientific), and RNA was extracted using the RNeasy Mini Kit (Qiagen, Hilden, Germany). After reverse transcription using Maxima H Minus RT (Thermo Fisher Scientific) with Oligo(dT) primers, qPCR was performed using SYBRgreen (Thermo Fisher Scientific) on a BioRad CFX cycler using the following primers:

N-241 (5′→3′ TTACCACTCGATCCAGACTTC)

N-331+ (5′→3′ CCTATTAGTGCCCCTGTTAGTTT)

Flow cytometry of tumors and tumor-draining lymph nodes

Freshly explanted tumors or tumor-draining lymph nodes were transferred into appropriately sized tubes with D-PBS, stored on ice, and processed on the same day. The collected samples were minced in small pieces in RPMI-1640 + 10% FCS + 200 U/mL collagenase type I (Thermo Fisher Scientific), transferred into 50 mL tubes, and incubated at 37°C for 30 min with gentle vortexing every 10 min. The obtained suspensions were passed through 100 μm cell strainers, spun down at 300 × *g* for 5 min, and resuspended in 10 mL D-PBS. The cells were counted, and 2×10^6 cells per sample were used for antibody staining in 100 μL D-PBS. For analysis of T and NK cell abundance and activation, the tumor samples were stained with fluorochrome-conjugated antibodies against the following murine lymphocyte markers: 1 μL CD45.2-PerCP-Cy™5.5 (clone 104), 1 μL CD4-APC-Cy™7 (clone GK1.5), 1 μL CD8a-APC (clone 53-6.7) (all from BD Biosciences), 1.25 μL CD69-PE (clone H1.2F3), and 2 μL CD335-FITC (clone 29A1.4) (both from BioLegend). For analysis of memory T cell populations, the tumor samples and tumor-draining lymph node samples were stained with following antibodies: 1 μL CD3-PerCP-Cy™5.5 (clone 17A2), 1 μL CD4-APC-Cy™7 (clone GK1.5), 1 μL CD8a-APC (clone 53-6.7) (all from BD Biosciences), 1 μL CD44-PE (clone IM7), and 1 μL CD62L-FITC (clone MEL-14) (both from BioLegend). After incubation in the dark for 30 min, 1 mL D-PBS was added per sample, and samples were spun down for 5 min at 300 × *g*. The pellets were resuspended in 500 μL D-PBS with 0.2 μg/mL DAPI. Directly afterward, the samples were acquired on a BD FACS LSR II (BD Biosciences). Data were analyzed using FlowJo software. Only samples with at least 1,000 cells were included in the analysis.

Tumor-specific IFN-γ restimulation assay

The detailed protocol for IFN-γ restimulation assay has been described previously.[61] In brief, MC38 cells were resuspended in RPMI + 10% FCS + 1% penicillin/streptomycin + 20 U/mL IL-2 +

20 μg/mL mitomycin-C and incubated for 2 h with shaking at 37°C. Afterward, the cells were washed three times with D-PBS and resuspended in RPMI-1640 with 10% FCS, 1% penicillin/streptomycin, and 20 U/mL recombinant interleukin-2 (IL-2). In parallel, single-cell suspensions were prepared from freshly isolated murine spleens. The spleens were meshed through a 100 μm cell strainer (Neolab, Heidelberg, Germany) into 10 mL D-PBS. The obtained suspension was then centrifuged at 300 × *g* for 5 min at RT. The supernatant was discarded, and the cell pellet was resuspended in 1 mL ACK Lysing buffer (Thermo Fisher Scientific) and incubated for 10 min at RT. After the incubation, 9 mL D-PBS were added per sample and centrifuged at 300 × *g* for 5 min. The resulting pellet was resuspended in D-PBS, and cells were counted. Cocultures were prepared in RPMI-1640 + 10% FCS + 1% penicillin/streptomycin + 20 U/mL IL-2 using 1.7×10^5 MC38 tumor cells treated with mitomycin C and 5×10^6 splenocytes in a total volume of 1 mL in 24-well plates and incubated at 37°C and 5% CO_2. Medium was collected after 48 h and stored at −80°C until analysis. IFN-γ concentration was measured in the collected samples using an IFN-γ Mouse Uncoated ELISA Kit (Thermo Fisher Scientific).

ELISA for αmPD-1, pembrolizumab, and nivolumab

ELISA plates (Nunc Maxisorp) were coated with 100 ng per well recombinant mouse or human PD-1, His-tagged (Sinobiological, Beijing, China) overnight at 4°C. Wells were washed twice with D-PBS, and blocking buffer (PBS + 5% FCS + 0.05% Tween 20) was added for 2 h at RT. After washing three times with D-PBS, 100 μL samples were added for 2 h at RT. Following four washes with washing buffer (D-PBS + 0.05% Tween 20), 100 μL of diluted Biotin-coupled goat anti-hamster IgG (H + L) Secondary Antibody (Thermo Fisher Scientific; 1:20,000 in blocking buffer, for αmPD-1) or anti-human IgG4 antibody (Sigma-Aldrich; clone HP-6025, 1:60,000 in blocking buffer, for pembrolizumab and nivolumab) were added to each well and incubated for 1 h at RT. After five washing steps, 100 μL of diluted HRP-Streptavidin (Dianova, Hamburg, Germany; 1:500) was added per well and incubated for 10 min at RT. Wells were washed five times, and 100 μL of 1-Step Ultra TMB (Fisher Scientific) was added and incubated for ∼10 min at RT before addition of 100 μL Stop solution (Takara Bio, Shiga, Japan). Absorbance at 450 nm was determined using a microplate reader. Anti-mouse PD-1 (clone J43) was obtained from Thermo Fisher Scientific. Pembrolizumab and nivolumab as positive controls and standards were obtained from the Pharmacy of the University Hospital Heidelberg.

Functional assay for pembrolizumab and nivolumab

To assess the functionality of MeVac-encoded pembrolizumab and nivolumab, peripheral blood mononuclear cells were stimulated with the superantigen *Staphylococcus* enterotoxin B in an assay adapted from Wang et al.[62] Supernatants from mock infected cells, cells infected with MeVac IgG4-Fc, and MeVac encoding pembrolizumab or nivolumab were collected. Antibody concentrations were determined using ELISA as described above. PBMCs from healthy donors were isolated using Ficoll-Hypaque by density gradient centrifugation, and 5×10^5 cells per well were seeded into a 96-well plate in RPMI + 5% human serum (Sigma-Aldrich). After overnight culture, SEB (Sigma-Aldrich) diluted in D-PBS was added at final concentrations of 20, 200, and 2,000 ng/mL. Cell culture supernatants from infected cells corresponding to 10 μg/mL pembrolizumab, nivolumab, or IgG4-Fc were added to respective wells. Forty and 70 h later, cell culture supernatants were collected, and IL-2 concentrations were determined using ELISA (IL-2 Human Uncoated ELISA kit; Thermo Fisher Scientific).

Statistical analyses and visualization

Statistical analyses were performed using GraphPad Prism version 8 (Graph Pad Software, San Diego, CA). The graphical abstract was created using BioRender.com.

SUPPLEMENTAL INFORMATION

Supplemental information can be found online at https://doi.org/10.1016/j.omto.2021.11.020.

ACKNOWLEDGMENTS

We acknowledge S. Russell, R. Cattaneo, A. Jassowicz, C. Plass, S. Eichmüller, and W. Osen for providing cell lines. We thank J. Albert, B. Hoyler, and S. Sawall for technical assistance. This work was funded by the German National Science Foundation (Deutsche Forschungsgemeinschaft, DFG, grant EN 1119/2–2 to C.E.E.), the Else Kröner-Fresenius-Stiftung (2019_EKMS.02 to C.E.E.), and the Wilhelm Sander-Stiftung (grant 2018.058.1 to C.E.E.). R.V. was supported by a scholarship from the Heidelberg School of Oncology (HSO) and by the European Regional Development Fund (ERDF) project no. 1.1.1.2/VIAA/2/18/292. G.P.-M. received a scholarship from the Helmholtz International Graduate School for Cancer Research.

AUTHOR CONTRIBUTIONS

Conceptualization, C.E.E. and R.V.; Methodology, R.V.; Investigation and Analyses, R.V., G.P.-M., C.M., L.M.J., and L.K.; Writing – Original Draft: R.V. and C.E.E.; Writing – Review & Editing: G.P.-M., R.V., L.M.J., and C.E.E.; Resources, G.U., C.J.B., and D.J.

DECLARATION OF INTERESTS

G.U. is a co-founder, stakeholder, and chief medical officer (CMO)/chief scientific officer (CSO) of CanVirex AG, a company investigating oncolytic viruses as cancer immunotherapeutics.

REFERENCES

1. Pardoll, D.M. (2012). The blockade of immune checkpoints in cancer immunotherapy. Nat. Rev. Cancer *12*, 252–264.
2. Ribas, A., and Wolchok, J.D. (2018). Cancer immunotherapy using checkpoint blockade. Science *359*, 1350–1355.
3. Sharpe, A.H., and Pauken, K.E. (2018). The diverse functions of the PD1 inhibitory pathway. Nat. Rev. Immunol. *18*, 153–167.
4. Okazaki, T., and Honjo, T. (2007). PD-1 and PD-1 ligands: from discovery to clinical application. Int. Immunol. *19*, 813–824.
5. Chamoto, K., Hatae, R., and Honjo, T. (2020). Current issues and perspectives in PD-1 blockade cancer immunotherapy. Int. J. Clin. Oncol. *25*, 790–800.

6. Nowicki, T.S., Hu-Lieskovan, S., and Ribas, A. (2018). Mechanisms of resistance to PD-1 and PD-L1 blockade. Cancer J. *24*, 47–53.
7. Tumeh, P.C., Harview, C.L., Yearley, J.H., Shintaku, I.P., Taylor, E.J., Robert, L., Chmielowski, B., Spasic, M., Henry, G., Ciobanu, V., et al. (2014). PD-1 blockade induces responses by inhibiting adaptive immune resistance. Nature *515*, 568–571.
8. Michot, J.M., Bigenwald, C., Champiat, S., Collins, M., Carbonnel, F., Postel-Vinay, S., Berdelou, A., Varga, A., Bahleda, R., Hollebecque, A., et al. (2016). Immune-related adverse events with immune checkpoint blockade: a comprehensive review. Eur. J. Cancer *54*, 139–148.
9. Achard, C., Surendran, A., Wedge, M.E., Ungerechts, G., Bell, J., and Ilkow, C.S. (2018). Lighting a fire in the tumor microenvironment using oncolytic immunotherapy. EBioMedicine *31*, 17–24.
10. Liu, Z., Ravindranathan, R., Kalinski, P., Guo, Z.S., and Bartlett, D.L. (2017). Rational combination of oncolytic vaccinia virus and PD-L1 blockade works synergistically to enhance therapeutic efficacy. Nat. Commun. *8*, 14754.
11. Goepfert, K., Dinsart, C., Rommelaere, J., Foerster, F., and Moehler, M. (2019). Rational combination of parvovirus H1 with CTLA-4 and PD-1 checkpoint inhibitors dampens the tumor induced immune silencing. Front Oncol. *9*, 425.
12. Engeland, C.E., Grossardt, C., Veinalde, R., Bossow, S., Lutz, D., Kaufmann, J.K., Shevchenko, I., Umansky, V., Nettelbeck, D.M., Weichert, W., et al. (2014). CTLA-4 and PD-L1 checkpoint blockade enhances oncolytic measles virus therapy. Mol. Ther. *22*, 1949–1959.
13. McGray, A.J.R., Huang, R.Y., Battaglia, S., Eppolito, C., Miliotto, A., Stephenson, K.B., Lugade, A.A., Webster, G., Lichty, B.D., Seshadri, M., et al. (2019). Oncolytic Maraba virus armed with tumor antigen boosts vaccine priming and reveals diverse therapeutic response patterns when combined with checkpoint blockade in ovarian cancer. J. Immunother. Cancer *7*, 189.
14. Rajani, K., Parrish, C., Kottke, T., Thompson, J., Zaidi, S., Ilett, L., Shim, K.G., Diaz, R.M., Pandha, H., Harrington, K., et al. (2016). Combination therapy with reovirus and anti-PD-1 blockade controls tumor growth through innate and adaptive immune responses. Mol. Ther. *24*, 166–174.
15. Ribas, A., Dummer, R., Puzanov, I., VanderWalde, A., Andtbacka, R.H.I., Michielin, O., Olszanski, A.J., Malvehy, J., Cebon, J., Fernandez, E., et al. (2018). Oncolytic virotherapy promotes intratumoral T cell infiltration and improves anti-PD-1 immunotherapy. Cell *174*, 1031–1032.
16. Sun, L., Funchain, P., Song, J.M., Rayman, P., Tannenbaum, C., Ko, J., McNamara, M., Marcela Diaz-Montero, C., and Gastman, B. (2018). Talimogene laherparepvec combined with anti-PD-1 based immunotherapy for unresectable stage III-IV melanoma: a case series. J. Immunother. Cancer *6*, 36.
17. Sivanandam, V., LaRocca, C.J., Chen, N.G., Fong, Y., and Warner, S.G. (2019). Oncolytic viruses and immune checkpoint inhibition: the best of both worlds. Mol. Ther. Oncolytics *13*, 93–106.
18. Engeland, C.E., and Ungerechts, G. (2021). Measles virus as an oncolytic immunotherapy. Cancers *13*, 544.
19. Galanis, E., Hartmann, L.C., Cliby, W.A., Long, H.J., Peethambaram, P.P., Barrette, B.A., Kaur, J.S., Haluska, P.J., Jr., Aderca, I., Zollman, P.J., et al. (2010). Phase I trial of intraperitoneal administration of an oncolytic measles virus strain engineered to express carcinoembryonic antigen for recurrent ovarian cancer. Cancer Res. *70*, 875–882.
20. Galanis, E., Atherton, P.J., Maurer, M.J., Knutson, K.L., Dowdy, S.C., Cliby, W.A., Haluska, P., Jr., Long, H.J., Oberg, A., Aderca, I., et al. (2015). Oncolytic measles virus expressing the sodium iodide symporter to treat drug-resistant ovarian cancer. Cancer Res. *75*, 22–30.
21. Russell, S.J., Federspiel, M.J., Peng, K.W., Tong, C., Dingli, D., Morice, W.G., Lowe, V., O'Connor, M.K., Kyle, R.A., Leung, N., et al. (2014). Remission of disseminated cancer after systemic oncolytic virotherapy. Mayo Clin. Proc. *89*, 926–933.
22. Dispenzieri, A., Tong, C., LaPlant, B., Lacy, M.Q., Laumann, K., Dingli, D., Zhou, Y., Federspiel, M.J., Gertz, M.A., Hayman, S., et al. (2017). Phase I trial of systemic administration of Edmonston strain of measles virus genetically engineered to express the sodium iodide symporter in patients with recurrent or refractory multiple myeloma. Leukemia *31*, 2791–2798.
23. Packiriswamy, N., Upreti, D., Zhou, Y., Khan, R., Miller, A., Diaz, R.M., Rooney, C.M., Dispenzieri, A., Peng, K.W., and Russell, S.J. (2020). Oncolytic measles virus therapy enhances tumor antigen-specific T-cell responses in patients with multiple myeloma. Leukemia *34*, 3310–3322.
24. Veinalde, R., Grossardt, C., Hartmann, L., Bourgeois-Daigneault, M.C., Bell, J.C., Jäger, D., von Kalle, C., Ungerechts, G., and Engeland, C.E. (2017). Oncolytic measles virus encoding interleukin-12 mediates potent antitumor effects through T cell activation. Oncoimmunology *6*, e1285992.
25. Hardcastle, J., Mills, L., Malo, C.S., Jin, F., Kurokawa, C., Geekiyanage, H., Schroeder, M., Sarkaria, J., Johnson, A.J., and Galanis, E. (2017). Immunovirotherapy with measles virus strains in combination with anti-PD-1 antibody blockade enhances antitumor activity in glioblastoma treatment. Neuro Oncol. *19*, 493–502.
26. Speranza, M.C., Passaro, C., Ricklefs, F., Kasai, K., Klein, S.R., Nakashima, H., Kaufmann, J.K., Ahmed, A.K., Nowicki, M.O., Obi, P., et al. (2018). Preclinical investigation of combined gene-mediated cytotoxic immunotherapy and immune checkpoint blockade in glioblastoma. Neuro Oncol. *20*, 225–235.
27. Dekkers, G., Bentlage, A.E.H., Stegmann, T.C., Howie, H.L., Lissenberg-Thunnissen, S., Zimring, J., Rispens, T., and Vidarsson, G. (2017). Affinity of human IgG subclasses to mouse Fc gamma receptors. MAbs *9*, 767–773.
28. Ungerechts, G., Springfeld, C., Frenzke, M.E., Lampe, J., Parker, W.B., Sorscher, E.J., and Cattaneo, R. (2007). An immunocompetent murine model for oncolysis with an armed and targeted measles virus. Mol. Ther. *15*, 1991–1997.
29. Hammond, A.L., Plemper, R.K., Zhang, J., Schneider, U., Russell, S.J., and Cattaneo, R. (2001). Single-chain antibody displayed on a recombinant measles virus confers entry through the tumor-associated carcinoembryonic antigen. J. Virol. *75*, 2087–2096.
30. Reul, J., Frisch, J., Engeland, C.E., Thalheimer, F.B., Hartmann, J., Ungerechts, G., and Buchholz, C.J. (2019). Tumor-specific delivery of immune checkpoint inhibitors by engineered AAV vectors. Front Oncol. *9*, 52.
31. Upadhaya, S., Neftelino, S.T., Hodge, J.P., Oliva, C., Campbell, J.R., and Yu, J.X. (2021). Combinations take centre stage in PD1/PDL1 inhibitor clinical trials. Nat. Rev. Drug Discov. *20*, 168–169.
32. Lichty, B.D., Breitbach, C.J., Stojdl, D.F., and Bell, J.C. (2014). Going viral with cancer immunotherapy. Nat. Rev. Cancer *14*, 559–567.
33. Twumasi-Boateng, K., Pettigrew, J.L., Kwok, Y.Y.E., Bell, J.C., and Nelson, B.H. (2018). Oncolytic viruses as engineering platforms for combination immunotherapy. Nat. Rev. Cancer *18*, 419–432.
34. Tanoue, K., Rosewell Shaw, A., Watanabe, N., Porter, C., Rana, B., Gottschalk, S., Brenner, M., and Suzuki, M. (2017). Armed oncolytic adenovirus-expressing PD-L1 mini-body enhances antitumor effects of chimeric antigen receptor T cells in solid tumors. Cancer Res. *77*, 2040–2051.
35. Saha, D., Martuza, R.L., and Rabkin, S.D. (2017). Macrophage polarization contributes to glioblastoma eradication by combination immunovirotherapy and immune checkpoint blockade. Cancer Cell *32*, 253–267.e255.
36. Yadav, M., Jhunjhunwala, S., Phung, Q.T., Lupardus, P., Tanguay, J., Bumbaca, S., Franci, C., Cheung, T.K., Fritsche, J., Weinschenk, T., et al. (2014). Predicting immunogenic tumour mutations by combining mass spectrometry and exome sequencing. Nature *515*, 572–576.
37. Polesso, F., Munks, M.W., Rott, K.H., Smart, S., Hill, A.B., and Moran, A.E. (2021). PD-1-specific "Blocking" antibodies that deplete PD-1(+) T cells present an inconvenient variable in preclinical immunotherapy experiments. Eur. J. Immunol. *51*, 1473–1481.
38. Chen, X., Song, X., Li, K., and Zhang, T. (2019). FcγR-binding is an important functional attribute for immune checkpoint antibodies in cancer immunotherapy. Front Immunol. *10*, 292.
39. Monjazeb, A.M., Wang, Z., Vick, L.V., Dunai, C., Minnar, C., Khuat, L.T., and Murphy, W.J. (2021). Mouse preclinical cancer immunotherapy modeling involving anti-PD-1 therapies reveals the need to use mouse reagents to mirror clinical paradigms. Cancers *13*, 729.
40. Fransen, M.F., Schoonderwoerd, M., Knopf, P., Camps, M.G., Hawinkels, L.J., Kneilling, M., van Hall, T., and Ossendorp, F. (2018). Tumor-draining lymph nodes are pivotal in PD-1/PD-L1 checkpoint therapy. JCI Insight *3*, e124507.
41. Dammeijer, F., van Gulijk, M., Mulder, E.E., Lukkes, M., Klaase, L., van den Bosch, T., van Nimwegen, M., Lau, S.P., Latupeirissa, K., Schetters, S., et al. (2020). The PD-1/

PD-L1-checkpoint restrains T cell immunity in tumor-draining lymph nodes. Cancer Cell *38*, 685–700.e688.

42. Welstead, G.G., Iorio, C., Draker, R., Bayani, J., Squire, J., Vongpunsawad, S., Cattaneo, R., and Richardson, C.D. (2005). Measles virus replication in lymphatic cells and organs of CD150 (SLAM) transgenic mice. Proc. Natl. Acad. Sci. U S A. *102*, 16415–16420.

43. Backhaus, P.S., Veinalde, R., Hartmann, L., Dunder, J.E., Jeworowski, L.M., Albert, J., Hoyler, B., Poth, T., Jäger, D., Ungerechts, G., et al. (2019). Immunological effects and viral gene expression determine the efficacy of oncolytic measles vaccines encoding IL-12 or IL-15 agonists. Viruses *11*, 914.

44. Veinalde, R., Pidelaserra-Marti, G., Heidbuechel, J.P., Kang, N., Abate-Daga, D., Ball, C.R., Ungerechts, G., and Engeland, C.E. (2019). Translational research on synergy of PD-1 checkpoint blockade and oncolytic measles virotherapy. Mol. Ther. *27*, 124.

45. Borcoman, E., Kanjanapan, Y., Champiat, S., Kato, S., Servois, V., Kurzrock, R., Goel, S., Bedard, P., and Le Tourneau, C. (2019). Novel patterns of response under immunotherapy. Ann. Oncol. *30*, 385–396.

46. Hsu, J., Hodgins, J.J., Marathe, M., Nicolai, C.J., Bourgeois-Daigneault, M.C., Trevino, T.N., Azimi, C.S., Scheer, A.K., Randolph, H.E., Thompson, T.W., et al. (2018). Contribution of NK cells to immunotherapy mediated by PD-1/PD-L1 blockade. J. Clin. Invest *128*, 4654–4668.

47. Pitt, J.M., Vétizou, M., Daillère, R., Roberti, M.P., Yamazaki, T., Routy, B., Lepage, P., Boneca, I.G., Chamaillard, M., Kroemer, G., et al. (2016). Resistance mechanisms to immune-checkpoint blockade in cancer: tumor-intrinsic and -extrinsic factors. Immunity *44*, 1255–1269.

48. Speck, T., Heidbuechel, J.P.W., Veinalde, R., Jaeger, D., von Kalle, C., Ball, C.R., Ungerechts, G., and Engeland, C.E. (2018). Targeted BiTE expression by an oncolytic vector augments therapeutic efficacy against solid tumors. Clin. Cancer Res. *24*, 2128–2137.

49. Keenan, T.E., Burke, K.P., and Van Allen, E.M. (2019). Genomic correlates of response to immune checkpoint blockade. Nat. Med. *25*, 389–402.

50. Kalbasi, A., and Ribas, A. (2020). Tumour-intrinsic resistance to immune checkpoint blockade. Nat. Rev. Immunol. *20*, 25–39.

51. Nakamura, T., Peng, K.W., Harvey, M., Greiner, S., Lorimer, I.A., James, C.D., and Russell, S.J. (2005). Rescue and propagation of fully retargeted oncolytic measles viruses. Nat. Biotechnol. *23*, 209–214.

52. Robbins, P.F., Kantor, J.A., Salgaller, M., Hand, P.H., Fernsten, P.D., and Schlom, J. (1991). Transduction and expression of the human carcinoembryonic antigen gene in a murine colon carcinoma cell line. Cancer Res. *51*, 3657–3662.

53. Lei, J., Osen, W., Gardyan, A., Hotz-Wagenblatt, A., Wei, G., Gissmann, L., Eichmüller, S., and Löchelt, M. (2015). Replication-competent foamy virus vaccine vectors as novel epitope scaffolds for immunotherapy. PLoS One *10*, e0138458.

54. Samorski, R., Gissmann, L., and Osen, W. (2006). Codon optimized expression of HPV 16 E6 renders target cells susceptible to E6-specific CTL recognition. Immunol. Lett. *107*, 41–49.

55. Calain, P., and Roux, L. (1993). The rule of six, a basic feature for efficient replication of Sendai virus defective interfering RNA. J. Virol. *67*, 4822–4830.

56. Radecke, F., Spielhofer, P., Schneider, H., Kaelin, K., Huber, M., Dötsch, C., Christiansen, G., and Billeter, M.A. (1995). Rescue of measles viruses from cloned DNA. Embo j *14*, 5773–5784.

57. Martin, A., Staeheli, P., and Schneider, U. (2006). RNA polymerase II-controlled expression of antigenomic RNA enhances the rescue efficacies of two different members of the Mononegavirales independently of the site of viral genome replication. J. Virol. *80*, 5708–5715.

58. Heidbuechel, J.P.W., and Engeland, C.E. (2019). Paramyxoviruses for tumor-targeted Immunomodulation: design and evaluation ex vivo. J. Vis. Exp. *143*, e58651.

59. Rueden, C.T., Schindelin, J., Hiner, M.C., DeZonia, B.E., Walter, A.E., Arena, E.T., and Eliceiri, K.W. (2017). ImageJ2: ImageJ for the next generation of scientific image data. BMC Bioinformatics *18*, 529.

60. Amsen, D., de Visser, K.E., and Town, T. (2009). Approaches to determine expression of inflammatory cytokines. Methods Mol. Biol. *511*, 107–142.

61. Veinalde, R. (2020). Evaluation of oncolytic virus-induced therapeutic tumor vaccination effects in murine tumor models. In Oncolytic Viruses, 2019/09/06 Edn, *2058*, C.E. Engeland, ed. (Humana), pp. 213–227.

62. Wang, C., Thudium, K.B., Han, M., Wang, X.T., Huang, H., Feingersh, D., Garcia, C., Wu, Y., Kuhne, M., Srinivasan, M., et al. (2014). In vitro characterization of the anti-PD-1 antibody nivolumab, BMS-936558, and in vivo toxicology in non-human primates. Cancer Immunol. Res. *2*, 846–856.